25. Fireman, E. L. & Langway, C. C. Jr Search for aluminum-26 in dust from the Greenland ice sheet. *Geochim. Cosmochim. Acta* **29,** 21–27 (1965).
26. Grun, E., Zook, H. A., Fechtig, H. & Geise, R. H. Collisional balance of the meteoritic complex. *Icarus* **62,** 244–272 (1985).
27. Lever, J. H., Taylor, S. & Harvey, R. P. A collector to retrieve micrometeorites from the South Pole water well. *Lunar Planet. Sci.* **XXVII,** 747–748 (1996).
28. Fluent Version 4.3, Fluent, Inc., Lebanon, New Hampshire 03766, USA (1995).
29. Lin, D. S. & Nansteel, M. W. Natural convection in a vertical annulus containing water near the density maximum. *J. Heat Transfer* **109,** 899–905 (1987).
30. Lankford, K. E. & Bejan, A. Natural convection in a vertical enclosure filled with water near 4 °C. *J. Heat Transfer* **108,** 755–763 (1986).

Acknowledgements. We thank J. Rand, J. Govoni and M. Shandrick for their help with our field work, and C. Engrand, D. Joswiak, S. Kuehner, D. Brownlee, M. Maurette, G. Kurat and C. Daghlian for their help with particle analysis. This work was supported by the National Science Foundation with additional support from CRREL.

Correspondence and requests for materials should be addressed to J.H.L. (e-mail: jlever@crrel.usace.army.mil).

Charge separation in localized and delocalized electronic states in polymeric semiconductors

A. Köhler*, D. A. dos Santos†, D. Beljonne†, Z. Shuai†, J.-L. Brédas†, A. B. Holmes‡, A. Kraus§, K. Müllen§ & R. H. Friend*

* *Cavendish Laboratory, University of Cambridge, Madingley Road, Cambridge CB3 0HE, UK*
† *Service de Chimie des Matériaux Nouveaux, Centre de Recherche en Electronique et Photonique Moléculaires, Université de Mons-Hainaut, Place du Parc, 20, B-7000 Mons, Belgium*
‡ *University Chemical Laboratory, Lensfield Road, Cambridge CB2 1EW, UK*
§ *Max-Planck-Institut für Polymerforschung, Ackermannweg 10, 55128 Mainz, Germany*

Conjugated polymers such as poly(*p*-phenylene vinylene)s (PPVs) allow low-cost fabrication of thin semiconducting films by solution processing onto substrates. Several polymeric optoelectronic devices have been developed in recent years, including field-effect transistors[1], light-emitting diodes[2], photocells[3,4] and lasers[5]. It is still not clear, however, whether the description of electronic excitations in these materials is most appropriately formulated within a molecular or semiconductor (band-theory) picture. In the former case, excited states are localized and are described as excitons; in the latter they are delocalized and described as free electron–hole pairs. Here we report studies of the electronic states associated with optical excitations in the visible and ultraviolet range for the conjugated polymer poly(2-methoxy-5-(2′-ethyl-hexyloxy)-*p*-phenylene vinylene) (MEH-PPV), by means of photocurrent measurements and quantum-chemical calculations. We find several photocurrent spectral features between 3 and 5 eV which are coupled with bands in the absorption spectrum. On modelling the excited states in this energy range, we have discovered an important feature that is likely to be general for materials composed of coupled molecular units: that mixing of delocalized conduction- and valence-band states with states localized on the molecular units produces a sequence of excited states in which positive and negative charges can be separated further at higher energies. In other words, these excited states facilitate charge separation, and provide a conceptual bridge between the molecular (localized) and semiconductor (delocalized) pictures.

An indication of the difficulty in finding a coherent description for polymeric materials which show both molecular and semiconductor properties is provided by the conflicting descriptions of polymer photoexcitations in the literature, ranging from 'free-electron' models[6] to localized excitons[7–9]. The question of how to describe such photoexcitations is not of merely academic interest, but determines the possible efficiency of polymer light-emitting diodes[2], diode lasers and photocells[3] and can provide clues for the understanding of long-distance (>10 Å) electron-transfer processes that are discussed as possible within a DNA matrix and might play a role in the mechanisms of DNA damage and repair processes[10,11].

Our present photocurrent measurements on MEH-PPV (Fig. 1)

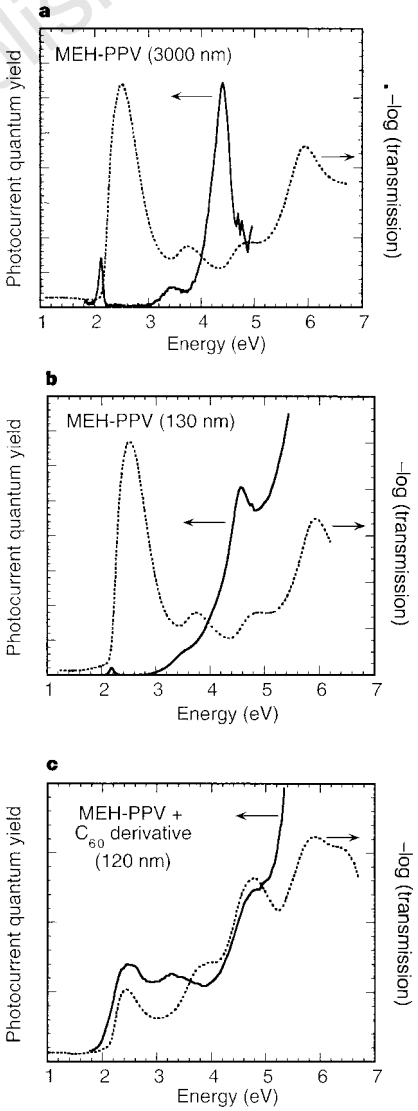

Figure 2 Short-circuit photocurrent spectra (solid line) and absorption spectra (dotted line) of different films. **a**, MEH-PPV (film thickness 3,000 nm); **b**, MEH-PPV (film thickness 130 nm); and **c**, a blend of 50 wt% MEH-PPV and the C_{60} derivative. For **c**, an indium tin oxide (ITO) electrode was used instead of gold, and illumination was through the semitransparent aluminium electrode. Intensities are given in arbitrary units.

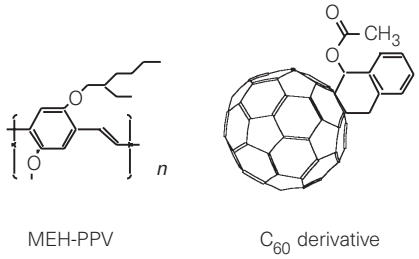

Figure 1 Structural formula of MEH-PPV and of the C_{60} derivative.

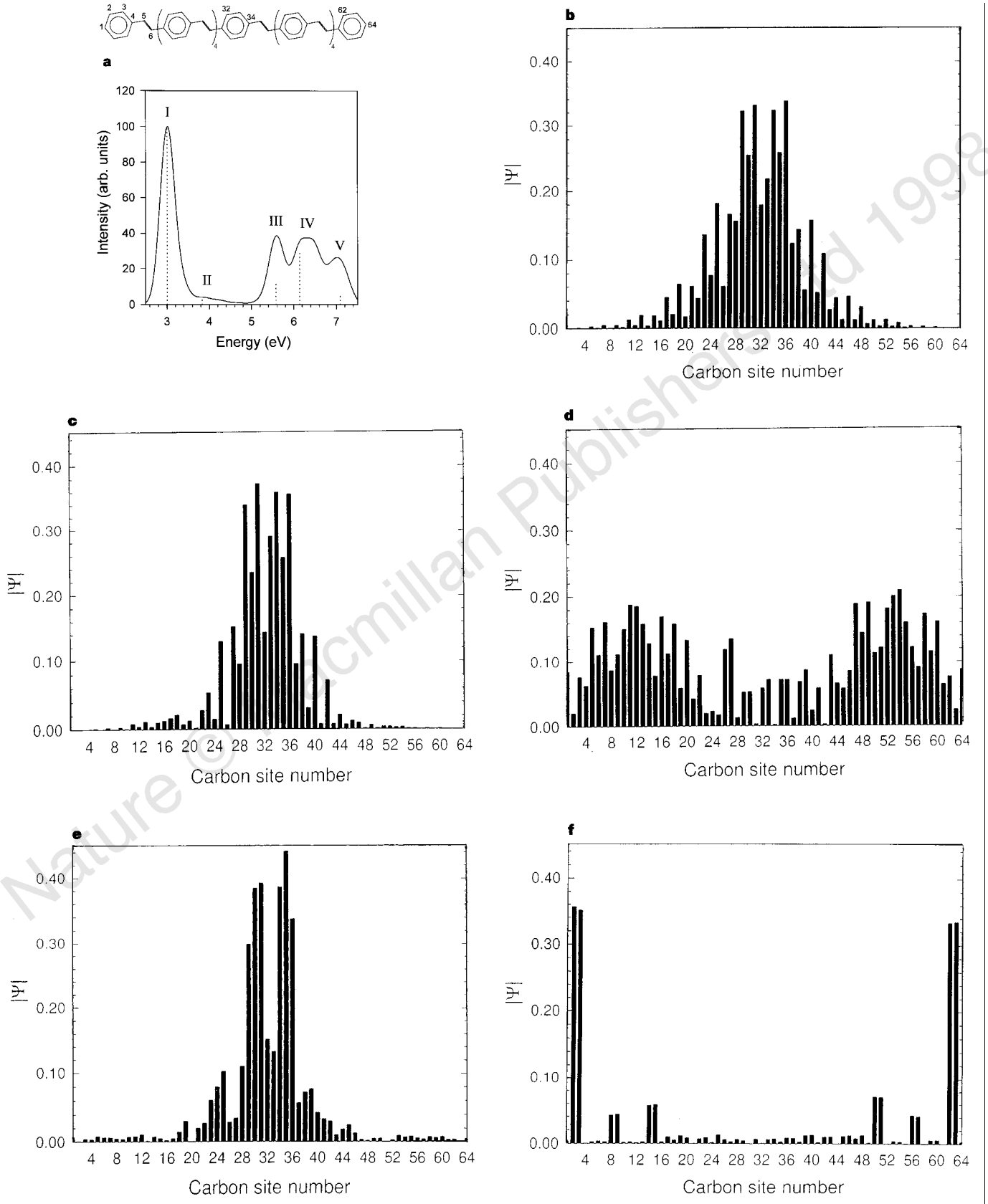

Figure 3 INDO/SCI calculations for the 11-ring PPV model oligomer; the site labelling is shown at the top. **a**, Simulated linear absorption spectrum. The vertical dotted lines represent the oscillator strength of the excited states for which the wavefunctions have been computed; the absolute value of the exciton wavefunction $|\Psi(x_e, x_h = 34)|$ calculated for the PPV undecamer as a function of carbon site for a fixed position of the hole at site 34 is shown for excitation into; **b**, the first absorption peak (3.1 eV); **c**, the second absorption peak (3.9 eV); **d**, the third absorption peak (4.8 eV); **e**, the fourth absorption peak (6.2 eV); and **f**, the fifth absorption peak (>6.5 eV). The energies given refer to the experimentally found peak positions. The corresponding theoretical transition energies (eV) are at 3.0, 3.8, 5.6, 6.3 and 7.0.

extend earlier reports[12,13] of the action spectrum for photodiodes and photoconduction spectra further into the ultraviolet, and allow comparison with the optical absorption spectra beyond the first π–π^* absorption band to cover three higher-lying absorption bands. The devices used for the photocurrent measurements were in the form of 'sandwich' structure diodes, fabricated in a layer structure of quartz substrate/semitransparent gold electrode/MEH-PPV film/semitransparent aluminium electrode. The short-circuit photocurrent was recorded in vacuum of 10^{-6} mbar. The photocurrent is corrected for the incident photon flux. Illumination was through the quartz substrate.

Figure 2a shows the photocurrent and absorption spectra of a photocell with a 3,000-nm-thick MEH-PPV film. The photocell was annealed at 100 °C for 12 h before the measurement to reduce the content of residual oxygen and water. We find photocurrent features at the onset of each absorption peak. In many photocells, we also observe a general photocurrent rise at and beyond 5 eV (Fig. 2b, for a 130-nm-thick MEH-PPV film, not annealed). We note that the third photocurrent feature is much larger than the first two. This increase in the photocurrent quantum yield does not scale with the size of the absorption coefficient, and cannot be accounted for by 'internal filter effects'[14–16]. For example, the absorption coefficient of MEH-PPV (Fig. 2b) is the same at 2.3 eV, 3.5 eV and 4.6 eV. Addition of an electron-accepting species such as a soluble C_{60} derivative[17] (to give a blend of 50 wt%, corresponding to one C_{60} derivative per four MEH-PPV repeat units) increases the intensity of the first two photocurrent features relative to the third feature in addition to giving an overall rise in the photocurrent quantum yield (Fig. 2c). The rise in quantum yield will also involve other, complex contributions not addressed here, including improved charge transport. The photocurrent quantum yields were $\sim 10^{-3}$% at the first photocurrent peak for MEH-PPV; a value of 7% was measured for the blend of MEH-PPV and the C_{60} derivative when illuminated through the indium tin oxide electrode at a photon energy of 2.5 eV. The feature common to all these devices is the presence of several distinct photocurrent features connected with the absorption peaks. This demonstrates the role of several distinct electronic transitions in the process of charge generation, with different efficiencies of charge separation.

There has been considerable work done to calculate the optical transitions in PPV and related materials, by including Coulomb interactions[13], and taking into account the full chemical structure of the polymer repeat unit[18,19]. To investigate the cause of the large photocurrent yields at high photon energies we have performed 'intermediate neglect of differential overlap' (INDO)/'single configuration interaction' (SCI) calculations of the exciton wavefunction for the 11-ring PPV oligomer. We have computed the exciton wavefunction $|\Psi_{PPV}(x_e, x_h = 34)|$, which represents the probability amplitude of finding an electron in a given site x_e assuming that the hole is located in the middle of the oligomer backbone, that is, on site $x_h = 34$ (see the site labelling in Fig. 3a). We note that all occupied and unoccupied π levels are taken into account, in contrast to our earlier calculations[18]. Figure 3a shows the INDO/SCI simulated linear absorption spectrum of the model oligomer; representative exciton wavefunctions for each of the five calculated absorption peaks (hereafter denoted I, II, III, IV and V) are shown in Fig. 3b–f. These absorption peaks arise from contributions of both delocalized and localized π wavefunctions: the wavefunctions are illustrated in Fig. 4. When the electronic wavefunction of the molecular orbital has nodes at the *para*-positions of the ring, that is, at those carbon atoms which link neighbouring rings, there is negligible delocalization of charges between neighbouring rings—the charges are confined or localized to their own ring. However, when the electronic wavefunction has its nodes orthogonal to the polymer axis, the carbon atoms at the *para*-position carry a high charge density. Charge can then delocalize between neighbouring rings and indeed over the whole chain.

From Fig. 3b–f, we can distinguish between two types of excited states. First, there are states where the wavefunction, $|\Psi_{PPV}(x_e, x_h = 34)|$, has a narrow gaussian shape, centred on the hole site and confined to the neighbouring repeat units. This is the case for the states created by excitation into first, second and fourth absorption peaks. In particular, we estimate the coherence length of the lowest excited species (peak I), responsible for the luminescent properties of the polymer, to be of the order of five phenyl rings, while peak IV corresponds to excitations that hardly extend over more than a monomer unit. We find that the electronic transitions to these states are polarized parallel to the chain, consistent with the results reported in refs 19 and 20. From the analysis of the configuration interaction expansion, we find that these excited states arise from excitations between the same types of orbitals, that is, from delocalized occupied orbitals to delocalized unoccupied orbitals (peaks I and II), or between occupied and unoccupied electronic levels that are both confined on the phenylene rings (peak IV). We note that the excited states belonging to peaks I and IV correspond, respectively, to the 'B' and 'D' transitions mentioned in ref. 19. These are the excited states for which we measure only a low photocurrent quantum yield.

Second, there are excited states, which we term charge-transfer states, where there is a finite probability of finding the electron and hole separated by a few phenylene rings. This is the case for the states formed by excitation into the third (III) and fifth (V) absorption peak. These states correspond to excitations polarized in the plane of the π-network, with strong contributions perpendicular to the chain axis, as also reported in refs 19 and 20. In contrast to the first kind of states, their configuration-interaction description involves only electronic transitions from delocalized occupied molecular orbitals to localized unoccupied levels and vice versa (the electron is in a delocalized band state and the hole is confined on a benzene ring or vice versa; excitations 'A' and 'C' in ref. 19). These are the excited states that give rise to a particularly large photocurrent.

Sub-picosecond time-resolved measurements of photoluminescence have shown that there is extremely rapid cooling of higher-energy excited states, so that emission is essentially from the lowest singlet excited state within 1 ps (refs 21, 22). Under these conditions, the probability of charge separation depends on the ability of electron and hole to separate at short times (possibly aided by extrinsic means[23–25]), before the lowest-lying, bound exciton is formed. We consider that this is facilitated in the higher-lying excitonic transitions when there is increased separation of electron and hole; this is particularly important for the third absorption band, as shown in Fig. 3. By addition of a high concentration of a highly electronegative compound, such as 50 wt% of a C_{60} derivative, efficient charge separation can also be achieved for peaks I and II. The increase in charge separation efficiency for excitation into

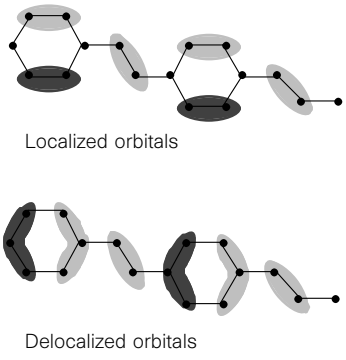

Figure 4 Scheme of molecular orbitals in poly(*p*-phenylene vinylene) with nodes at *para*-position and with nodes orthogonal to the molecular axis (after ref. 28). Different grey levels denote positive and negative signs of the molecular wavefunction.

Nature © Macmillan Publishers Ltd 1998

peak I can be used for the fabrication of efficient polymer photovoltaic cells[4].

In excited states that have their origin in a transition from a delocalized orbital to a delocalized orbital, both carriers, electron and hole, are similarly extended, and therefore spatially overlapped. The same is true for excited states that involve transitions from a localized orbital to another localized orbital. However, in an excited state formed by a transition from a localized orbital to a delocalized orbital, the hole is confined to the phenylene ring, while the electron is delocalized over the chain (or vice versa). We consider that this is the reason for the higher photocurrent yields of these states.

These results, which have antecedents in early work on molecular crystals (refs 25–27 and refs therein), have more general implications for the understanding of electronic excitations in low-dimensional systems[10,11]. The presence of charge-transfer states that separate more readily into free electron and holes can provide a natural description for the progression from molecular to semiconductor models of electronic excitations. □

Received 27 August 1997; accepted 23 February 1998.

1. Garnier, F., Hajlaoui, R., Yassar, A. & Srivastava, P. All-polymer field-effect transistor realized by printing techniques. *Science* **265,** 1684–1686 (1994).
2. Burroughes, J. H. *et al.* Light-emitting diodes based on conjugated polymers. *Nature* **347,** 539–541 (1990).
3. Halls, J. J. M. *et al.* Efficient photodiodes from interpenetrating polymer networks. *Nature* **376,** 498–500 (1995).
4. Yu, G., Gao, J., Hummelen, J. C., Wudl, F. & Heeger, A. J. Polymer photovoltaic cells: Enhanced efficiencies via a network of internal donor–acceptor heterojunctions. *Science* **270,** 1789–1791 (1995).
5. Tessler, N., Denton, G. J. & Friend, R. H. Lasing from conjugated-polymer microcavities. *Nature* **382,** 695–697 (1996).
6. Lee, C. H., Yu, G., Moses, D. & Heeger, A. J. Picosecond transient photoconductivity in poly(*p*-phenylenevinylene). *Phys. Rev. B* **49,** 2396–2407 (1994).
7. Heun, S. *et al.* Conformational effects in poly(*p*-phenylene vinylene) revealed by low-temperature site-selective fluorescence. *J. Phys.: Condens. Matter* **5,** 247–260 (1993).
8. Rauscher, U., Bässler, H., Bradley, D. D. C. & Hennecke, M. Exciton versus band description of the absorption and luminescence spectra in poly(para-phenylenevinylene). *Phys. Rev. B* **42,** 9830–9836 (1990).
9. Brédas, J. L., Cornil, J. & Heeger, A. J. The exciton binding energy in luminescent conjugated polymers. *Adv. Mater.* **8,** 447–452 (1996).
10. Fromherz, P. & Rieger, B. Photoinduced electron transfer in DNA matrix from intercalated ethidium to condensed methylviologen. *J. Am. Chem. Soc.* **108,** 5361–5362 (1986).
11. Hall, D. B., Holmlin, R. E. & Barton, J. K. Oxidative DNA damage through long-range electron transfer. *Nature* **382,** 731–735 (1996).
12. Pichler, K. *et al.* Optical spectroscopy of highly ordered poly(*p*-phenylene vinylene). *J. Phys.: Condens. Matter.* **5,** 7155–7172 (1993).
13. Chandross, M. *et al.* Excitons in poly(para-phenylenevinylene). *Phys. Rev. B* **50,** 14702–14705 (1994).
14. Tang, C. W. & Albrecht, A. C. Photovoltaic effects of metal-chlorophyll-metal sandwich cells. *J. Chem. Phys.* **62,** 2139–2149 (1974).
15. Marks, R. N., Halls, J. J. M., Bradley, D. D. C., Friend, R. H. & Holmes, A. B. The photovoltaic response in poly(*p*-phenylene vinylene) thin-film devices. *J. Phys.: Condens. Matter* **6,** 1379–1394 (1994).
16. Harrison, M. G., Grüner, J. & Spencer, G. C. W. Analysis of the photocurrent action spectra of MEH-PPV polymer photodiodes. *Phys. Rev. B* **55,** 7831–7849 (1997).
17. Kraus, A., Gügel, A., Belik, P., Walter, M. & Müllen, K. Covalent attachment of various substituents in closest proximity ot the C60-core: A broad synthetic approach to stable fullerene derivatives. *Tetrahedron* **51,** 9927–9940 (1996).
18. Cornil, J., Beljonne, D., Friend, R. H. & Brédas, J. L. Optical absorptions in poly(para-phenylene vinylene) and poly(2.5-dimethoxy-1,4-para-phenylene vinylene) oligomers. *Chem. Phys. Lett.* **223,** 82–88 (1994).
19. Gartstein, Y. N., Rice, M. J. & Conwell, E. M. Electron–hole interaction effects in the absorption-spectra of phenylene-based conjugated polymers. *Phys. Rev. B* **52,** 1683–1691 (1995).
20. Chandross, M. *et al.* Optical absorption in the substituted phenylene-based conjugated polymers: Theory and experiment. *Phys. Rev. B* **55,** 1486–1496 (1997).
21. Kersting, R. *et al.* Femtosecond energy relaxation in π-conjugated polymers. *Phys. Rev. Lett.* **70,** 3820–3823 (1993).
22. Hayes, G. H., Samuel, I. D. W. & Phillips, R. T. Exciton dynamics in electroluminescent polymers studied by femtosecond time-resolved photoluminescence spectroscopy. *Phys. Rev. B* **52,** R11569–R11572 (1995).
23. Harrison, N. T., Hayes, G. R., Phillips, R. T. & Friend, R. H. Singlet intrachain exciton generation and decay in poly(*p*-phenylenevinylene). *Phys. Rev. Lett.* **77,** 1881–1884 (1996).
24. Rothberg, L. J. *et al.* Intrinsic and extrinsic constrains on phenylenevinylene polymer electroluminescence. *Synth. Met.* **78,** 231–236 (1996).
25. Barth, S., Bässler, H., Rost, H. & Hörhold, H. H. Extrinsic and intrinsic dc photoconductivity in a conjugated polymer. *Phys. Rev. B* **56,** 3844–3851 (1997).
26. Pope, M. & Swenberg, C. E. *Electron Processes in Organic Crystals* (Clarendon, Oxford, 1982).
27. Gutmann, F. & Lyons, L. E. *Organic Semiconductors* (Wiley, New York, 1967).
28. Salaneck, W. R., Stafström, S. & Brédas, J.-L. *Conjugated Polymer Surfaces and Interfaces* (Cambridge Univ. Press, 1996).

Acknowledgements. We thank M. Harrison, S. Graham, P. Hamer and S. C. Moratti for discussions, and J. J. M. Halls for assistance with the UV photovoltaics equipment and for discussions. One of us (A.K.) thanks Wolfson College and Peterhouse in Cambridge for financial support. The Cambridge–Mons collaboration is supported by the European Commission (TMR Network 'SELOA' and ESPRIT project 'LEDFOS'). Work in Mons is partly supported by the Belgian Prime Minister Services for Scientific, Technical, and Cultural Affairs (IAP in Supramolecular Chemistry and Catalysis), FNRS-FRFC, and an IBM Academic Joint Study. D.B. is Chargé de Recherches FNRS.

Correspondence and requests for materials should be addressed to A.K. (e-mail: ak10007@cus.cam.ac.uk).

Current-limiting mechanisms in individual filaments extracted from superconducting tapes

X. Y. Cai*, A. Polyanskii*†, Q. Li‡, G. N. Riley Jr‡ & D. C. Larbalestier*

* *Applied Superconductivity Center, University of Wisconsin-Madison, Madison, Wisconsin 53706, USA*
† *Institute of Solid State Physics, Russian Academy of Science, 142432 Chernogolovka, Russia*
‡ *American Superconductor Corporation, Westborough, Massachusetts 01581, USA*

Many large-scale applications of high-temperature superconductors depend crucially on the ability to achieve high critical-current densities J_c (of the order of 10^5 A cm^{-2}). Existing silver-sheathed $(Bi,Pb)_2Sr_2Ca_2Cu_3O_x$ (BSCCO) tapes have J_c values that come within about 25% of this target[1–4], these values being limited by the fact that the supercurrent flows percolatively around barriers that occur over many length scales[5]. To elucidate the nature of these barriers, we have measured the transport properties of individual filaments extracted from very-high-J_c multifilament tapes[6]. We find that J_c for individual filaments reaches at least 8×10^4 A cm^{-2}—about 50% higher than the average value over the whole cross-section of the wire. Although we injected the current to flow along the crystallographic *a*–*b* planes of the material, we found that all filaments possessed local characteristics of *c*-axis transport, indicating the presence of occasional nanometre- to micrometre-scale barriers at basal-plane-faced grain boundaries. An independent and much larger limiting influence on the critical current comes from unhealed cracks produced by deformation during the processing of the wires. These results provide direct evidence that better processing methods aimed at improving the *c*-axis alignment and at inhibiting residual cracks should raise the accessible J_c values towards those needed for applications.

The filaments studied were extracted from an 85-filament, rectangular conductor, the J_c (at 77 K, 0 T) value of which was 54 kA cm^{-2}, averaged over the whole BSCCO cross-section. This value is characteristic of the very best conductor samples which can be made reproducibly[6]. The filaments, extracted by dissolving the silver away in a NH_4OH/H_2O solution, were 5–10 μm thick, 100–200 μm wide, and several millimetres long (Fig. 1a). Current leads were attached to both top and bottom faces with silver-epoxy to provide symmetric current feed into the *a*–*b* planes, as shown in Fig. 1a inset. Owing to filament burn-up in some of the first tests, sections between the voltage probes (~0.2 mm apart) were patterned into ~50-μm-wide bridges by slicing off the edges of the filaments with a laser-cutter (we admit the possibility that this may have removed the very highest-J_c regions of the filaments[7]).

Voltage–current characteristics were measured with a precision of ~10 nV. J_c was defined by I_c/A, where I_c is the critical current defined at the usual 1 μV cm^{-1} criterion and A is the minimum cross-sectional area of the filament between the voltage taps. Local variations in A which depend on the plate-like nature of the BSCCO grains produce local variations of the filament thickness of a few micrometres. Both thickness and width were measured with a light microscope to an accuracy of ~1 μm, making the width uncertain to ~5% and the thickness uncertain to 10–20%. J_c (77 K, 0 T) values obtained from seven different filaments ranged from 30 to 80 kA cm^{-2}, thus showing considerable macroscopic inhomogeneity